# Accepted Manuscript


An integrated experimental-theoretical approach to understand the electron transfer mechanism of adsorbed ferrocene-terminated alkanethiol monolayers

María F. Stragliotto, José L. Fernández, Sergio A. Dassie, Carla E. Giacomelli

PII: S0013-4686(17)32651-8

DOI: 10.1016/j.electacta.2017.12.091

Reference: EA 30879

To appear in: *Electrochimica Acta*

Received Date: 29 September 2017

Revised Date: 15 November 2017

Accepted Date: 12 December 2017

Please cite this article as: Marí.F. Stragliotto, José.L. Fernández, S.A. Dassie, C.E. Giacomelli, An integrated experimental-theoretical approach to understand the electron transfer mechanism of adsorbed ferrocene-terminated alkanethiol monolayers, *Electrochimica Acta* (2018), doi: 10.1016/j.electacta.2017.12.091.

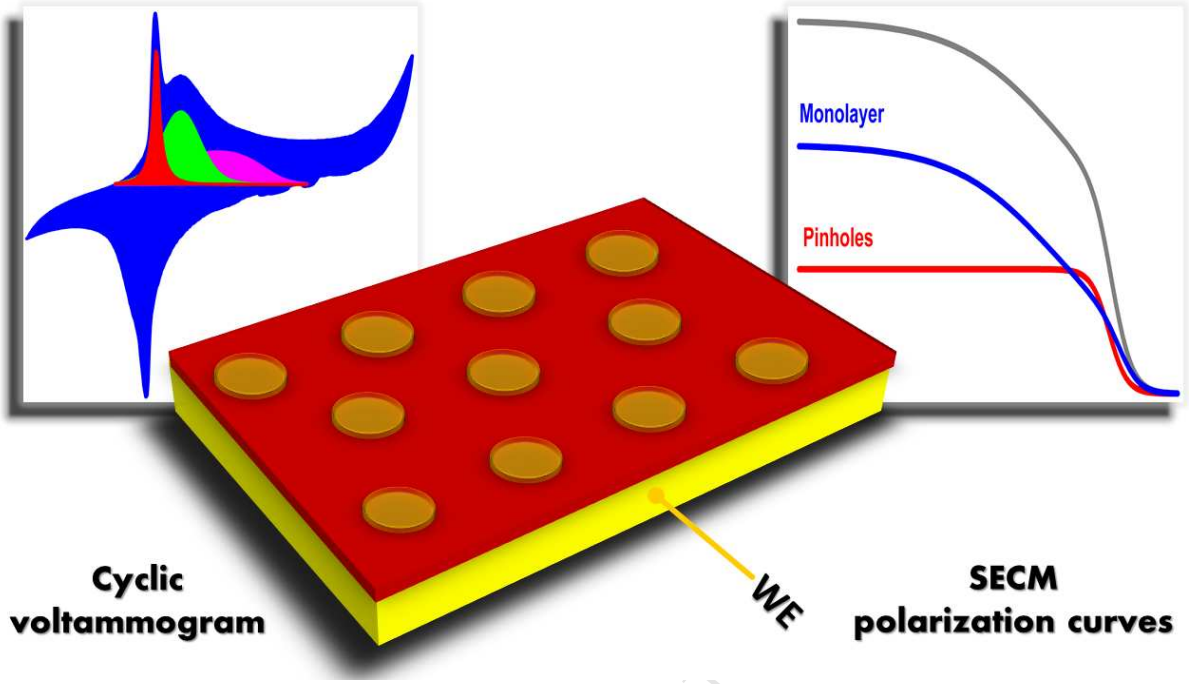

# An integrated experimental-theoretical approach to understand the electron transfer mechanism of adsorbed ferrocene-terminated alkanethiol monolayers

**María F. Stragliotto[1,2], José L. Fernández[3], Sergio A. Dassie[1,2], Carla E. Giacomelli[1,2,*]**

[1] Departamento de Fisicoquímica. Facultad de Ciencias Químicas. Universidad Nacional de Córdoba. Ciudad Universitaria. X5000HUA. Córdoba. Argentina.

[2] Instituto de Investigaciones en Fisicoquímica de Córdoba (INFIQC), CONICET. Ciudad Universitaria. X5000HUA. Córdoba. Argentina.

[3] IQAL and PRELINE. Facultad de Ingeniería Química. Universidad Nacional del Litoral. Santiago del Estero 2829. S3000AOM. Santa Fe. Argentina

*giacomel@fcq.unc.edu.ar*



## Abstract

In this work, the electron transfer mechanism of self-assembled monolayers of 6-ferrocenyl-1-hexanethiol (FcC6SH) on Au(111) substrates is addressed from two perspectives. To acquire a complete overview of the involved pathways, cyclic voltammetry and scanning electrochemical microscopy (SECM) were combined using an integrated experimental-theoretical approach. In the first case, the electrochemical behaviour is evaluated in the light of computer simulations of the experimental voltammetric response measured at successive potential scans in different supporting electrolytes. Successive potential scans change the lateral interactions between adsorbed Fc molecules that affect the oxidation of the electroactive monolayer. Furthermore, ion-pair formation between the oxidized ferrocene moieties and the anions of the supporting

electrolyte controls the electron transfer process as well as the type of the lateral interactions. In the second case, a thin-layer cell based formalism is used to develop a new model to understand feedback SECM experiments carried out with an additional redox mediator in solution. Since these experiments sense the parallel pathways of the electron transfer mechanism (pinholes and direct electron tunnelling and mediated electron transfer through the monolayer), the results are processed by using the new developed model for the analysis of the multipathway electron transfer mechanism. On that sense, the experimental results are processed by using the new SECM model accounting for the parallel electron transfer via the monolayer and the pinholes simultaneously.

**Keywords:**

Electroactive monolayer– 6-ferrocenyl-1-hexanethiol – Scanning Electrochemical Microscopy – Surface domains – TLC model

## 1. Introduction

Molecular structuring at interfaces has been booming since the late ‘90 due to the formation of self-assembled monolayers, preferably with thiolated molecules on gold substrates [1–5]. In particular, ferrocene-terminated alkanethiol (FcCnSH) molecules on gold substrates has provided with a simple and stable way to prepare tuneable films [4–6]. Furthermore, the presence of this electroactive moiety on the substrate has put forward significant advances to improve the protection against corrosion [7,8], to understand the electron transfer mechanisms [9–11], to enhance the performance of bioelectrochemical devices [12–16], and to exploit molecular electronics [17–22]. The stability of this surface modification relies on the strong interaction between the thiolated adsorbate and the gold substrate. However, the intermolecular interactions between adsorbed molecules play a key role in determining the energetics and kinetics of the adsorption and assembling processes. Therefore, the structure and dynamics of the interface are the result of different type of interactions involving the substrate, adsorbate and solvent molecules [1,5,23]. Considering that the FcCnSH molecules attached to gold substrates are mostly used as an electron transfer mediator, an externally applied potential can as well modulate these interactions [24]. In addition, the electrogenerated oxidized ferrocene ($Fc^+$) moieties at the interface can form ion-pairs with the anion of the supporting electrolyte[24–40]. Consequently, the nature and the concentration of the anion in solution have also an effect on the kinetics and thermodynamics of the redox reaction of FcCnSH modified gold substrates. In this scenery, the structure and dynamics of the electroactive monolayer can be modulated externally by the applied potential and the nature of the supporting electrolyte. Experimentally, the molecular structuring (i.e. the balance between the interactions involving the substrate, adsorbate molecules and ions of the supporting

electrolyte)strongly modifies the shape and the peak potential of the current-potential profiles [41,42].

Another important aspect that affects the electrochemical response of these FcCnSH modified gold substrates is the mechanism of electron transfer, which may involve many parallel pathways [43]. It is well known that direct electron tunnelling through the hydrocarbon chain can proceed on any type of monolayer on conducting substrates[44]. Moreover, electroactive monolayers with attached reduced ferrocene (Fc) moieties can also support mediated electron transfer through a serial mechanism involving bimolecular electron transfer between the redox center and the species in solution followed by electron transfer to/from the adsorbed FcCnSH molecules[45,46]. Recalling that monolayers are not perfectly ordered, particularly short alkyl chains ones[24,42], the electrochemical response is also strongly affected by the presence of pinholes in the monolayer ordering, as electron transfer can proceed directly on the gold substrate over these regions [43,47]. Precisely, electron transfer on these monolayer defects complicates the interpretation of electrochemical results, as an inappropriate uncoupling of this signal from the monolayer response generally leads to overestimated effective electron transfer rates [47].

Scanning electrochemical microscopy (SECM) has been successfully used to study the different pathways of the electron transfer mechanism through different thiolated monolayers on gold substrates [6,43,46–49]. In a typical feedback SECM experiment, the dependence of the tip current ($i_T$) on the tip-substrate distance ($d$) allows to estimate an effective rate constant ($k^{eff}$) for the electron transfer process through the Fc modified gold substrate to the tip-generated electroactive species in solution [48]. Then, the electron transfer mechanism can be evaluated from determining $k^{eff}$ values at different

operative variables, such as the substrate potential ($E_S$), the reactant concentration and the alkyl chain length. The kinetic parameters of the involved pathways can be estimated using specific theoretical formalisms developed for the SECM geometry [43,48]. However, the reported SECM studies on alkanethiol modified gold substrates have recognized the need to separate the responses from the pinholes to avoid the overestimation of $k^{eff}$. For instance, Bard and co-workers proposed that the contributions from the monolayer defects to the SECM feedback current quickly reach a diffusion-controlled regime [47]. According to this approach, the effect of pinholes on $i_T$ vs. $E_S$ curves at different *d* values leads to a constant current that can be subtracted from the global response to calculate $k^{eff}$ values for the electron transfer process through the monolayer [47].

In this work, the electron transfer mechanism of self-assembled monolayers of 6-ferrocenyl-1-hexanethiol (FcC6SH) on Au(111) substrates are addressed from two different perspectives: cyclic voltammetry and scanning electrochemical microscopy. In the first case, the electrochemical behaviour is evaluated in the light of computer simulations of the experimental voltammetric response measured at successive potential scans in different supporting electrolytes. The computer simulations were carried out using an integrated theoretical-experimental approach to analyse the nature of lateral interactions between adsorbed FcC6SH molecules in the monolayer. The simulations were performed applying a Laviron-type approach [50,51], similar to that used recently by Wandlowski and co-workers [52] and Yu and co-workers [53] to study the electrochemical behaviour of 11-ferrocenyl-1-undecanethiol (FcC11SH) self-assembled on gold. Further, the Laviron-type approach was also applied by Cao and co-workers to analyse the current-potential profiles of FcC6SH self-assembled on gold [16]. This

approach, not only represents a proof of concept to evaluate the coexistence of disordered regions with 2D patches or domains of locally ordered species on the gold substrate, but also a direct measure of the electron transfer between the redox moieties and the gold substrate. In the second case, an additional redox mediator is used in solution to sense the parallel pathways of the electron transfer mechanism (pinholes and direct electron tunnelling and mediated electron transfer through the monolayer). To understand feedback SECM experiments, a thin-layer cell (TLC)–based formalism was used as a benchmark to develop a model for the analysis of complete $i_T\left(E_S\right)$ curves at different *d* values. This formalism was originally proposed by Zoski and co-workers [54] and recently applied to analyse the hydrogen oxidation reaction mechanism [55]. The simplicity of the TLC configuration enables to model complex electron transfer processes without much difficulty. In fact, the experimental results (i.e. $i_T\left(E_S,d\right)$ curves) can be processed without intervention of any previous correction by using a SECM model accounting for the parallel electron transfer via the monolayer and pinholes simultaneously, as it was already proposed to analyse results from other electrochemical techniques. Thus for example, a very complete model proposed by Finklea et al. [44] to analyse polarization curves measured on alkanethiol modified electrodes not only considers the existence of clean (pinholes) and covered (perfectly ordered monolayer) sites, but also takes into account the presence of regions with collapsed monolayer around the pinholes. Notwithstanding, the incorporation of such a scheme in a SECM model for the interpretation of complete experimental $i_T\left(E_S,d\right)$ dependences requires a theoretical formalism different to that usually employed to correlate approach curves [43,46–48]. On that sense, the analysis of $i_T\left(E_S\right)$ over the whole $E_S$ range at different *d* values is carried out by using a versatile new theoretical

model that incorporates the substrate response operating in a TLC. The SECM model involves the simultaneous responses of the monolayer and pinholes for a simple reduction reaction and allows to understand the electron transfer process through the FcC6SH modified gold substrate to the tip-generated electroactive species. In short, this work combines thermodynamic and kinetic considerations to qualitatively improve the comprehension of the electron transfer mechanism of electroactive moieties anchored to conducting substrates.

## 2. Experimental Section

### *2.1. Chemicals and materials*

All reagents were of analytical grade and commercially available: $NaClO_4$, 6-ferrocenyl-1-hexanethiol (FcC6SH) and ferrocenemethanol (FcMeOH) from Sigma-Aldrich, $CH_2Cl_2$from Dorwil, KOH, $KH_2PO_4$ and $K_2HPO_4$ form Baker, $H_2SO_4$ from Cicarelli, and $HClO_4$ form Merck. All chemicals and solvents were used without further purification. The electrolyte solutions were prepared with ultrapure water (18 MΩ cm at 25 °C).

All the experiments were performed using the Au(111) substrate (either bare or modified) as working electrode, an Ag|AgCl|KCl (sat.) and a platinum wire were used as reference electrode and counter electrode, respectively. Platinum wires from Alfa Aesar and borosilicate capillaries from Paralwall (outer diameter: 1.4 mm, inner diameter: 1.1 mm) were used for the fabrication of SECM tips by a heat-sealing procedure described elsewhere [56].

*2.2. Instrumentation*

All the electrochemical measurements were performed using a potentiostat /galvanostat micro-Autolab PGSTAT 101 (Metrohm Autolab, The Netherlands) equipped with NOVA software at room temperature in a three-electrode cell.

SECM experiments were carried out using a home-built instrument described elsewhere [56]. The bipotentiostat was a PG 340 (Heka Elektronik, Germany) with an ITC-16 board. The tip position was controlled with three stepper motors (Zaber, Canada) and a Nanocube P-611.3S closed-loop XYZ nanopositioning system driven by an E-664 voltage amplifier/servo controller (Physik Instrumente, Germany). Both the bipotentiostat and the positioning system were commanded via the software Potmaster (Heka Elektronik).

*2.3. FcC6SH modified Au(111) substrates*

Gold on glass substrates (Arrandee®) were flame annealed prior to use by gentle heating with a butane torch and subsequently cooled down to room temperature in an nitrogen stream, a procedure known to produce Au(111) terraces [57]. These substrates were cleaned by immersion in hot piranha solution ($H_2O_2$-$H_2SO_4$ 1:3 mixture) for about 30 seconds (Caution! Piranha solution is a powerful oxidizing agent that reacts violently with most organic materials; it should be handled with extreme care). After that, the Au(111) substrates were rinsed with ultrapure water and further cleaned by cycling (50 successive scans) at 0.100 V $s^{-1}$ between 0.060 V and –1.400 V in 0.10 M KOH at room temperature. The substrate area exposed to the electrolyte was 0.33 $cm^2$, and the electroactive area was determined from the reduction gold signal measured in 0.10 M $H_2SO_4$ [58,59].

FcC6SH self-assembled monolayer was formed by dipping the Au(111) substrate in a 1.00 mM FcC6SH solution prepared in $CH_2Cl_2$ for 15 h at room temperature. The modified substrate was repeatedly rinsed with $CH_2Cl_2$ and ultrapure water prior to the electrochemical experiments.

*2.4. SECM experiments:*

SECM experiments were carried out in the feedback mode in which the cation ferricenium methanol ($FcMeOH^+$) in solution was generated under diffusion control at a Pt ultramicroelectrode-tip surface from FcMeOH. The tip-generated species interacts with the Fc modified gold substrate right under the tip and regenerates the mediator causing an increase of $i_T$ (so-called positive feedback). Steady-state $i_T(E_S)$ curves for the reduction of $FcMeOH^+$ were measured at different *d* values on a Fc modified Au(111) substrate in 1 mM FcMeOH solutions using 0.10 M $NaClO_4$ as supporting electrolyte.

Tip-substrate approach curves were measured with Pt tips at 0.40 V tip potential ($E_T$) and $E_S$ = –0.60 V. These approach curves were properly fitted with the theoretical expression for total positive feedback, which allowed to know *d* value during the acquisition of $i_T(E_S)$ curves. Once the tip was positioned at a certain *d* value, the steady state $i_T(E_S)$ curve was measured by a slow potentiodynamic scan at 0.010 V $s^{-1}$ of the $E_S$ from cathodic (–0.60 V) to anodic (0.40 V) values while keeping $E_T = 0.40\,\mathrm{V}$. After acquisition of a complete $i_T(E_S)$ curve the solution was agitated by a gentle

bubbling of air, *d* was changed using the piezo-positioner of the SECM instrument, and a new curve was measured.

## 3. Theory

### *3.1. Laviron-type approach*

The shape of the voltammograms were analysed using the Laviron-type approach [50,51], similar to that used recently by Wandlowski and co-workers [52], Yu and co-workers [53] and Cao and co-workers [16], that considers a random distribution of the electroactive species, a reversible electrochemical redox reaction, and strongly adsorbed oxidized (O) and reduced (R) species on the substrate. Furthermore, interactions between adsorbed molecules were modelled by a Frumkin-type isotherm. These interactions are assumed to be potential-independent, and an effective lateral interaction term G is defined as:

$$G = a_{OO} + a_{RR} - 2a_{OR} \tag{1}$$

where $a_{OO}$, $a_{RR}$ and $a_{OR}$ are the interaction constants between O-molecules, R-molecules and between them, respectively. The interaction constants are positive for the attraction forces while negative, for repulsions. The expression for the current-potential profiles is then [50]:

$$i = \left(\frac{F^2}{RT}\right) n^2 v A \Gamma_{\mathrm{T}} \frac{f(1-f)}{1 - 2\nu G \theta_{\mathrm{T}} f(1-f)} \tag{2}$$

where the potential dependence is expressed by the following equation [50]:

$$n\left(E - E_{\mathrm{peak}}\right) = \frac{RT}{F}\left[\ln\left(\frac{f}{1-f}\right) + \nu G \theta_{\mathrm{T}}(1-2f)\right] \tag{3}$$

where $\Gamma_T$ is the total adsorbed amount of the redox-active species; *n* is the number of electrons per oxidized/reduced molecule; *v* is the potential scan rate; $f = \theta_O/\theta_T$ ( $\theta_i = \Gamma_i/\Gamma_m$, being $\Gamma_m$ is the maximum adsorbed amount) is the fraction of the total coverage due to O-species, $\theta_T = \theta_O + \theta_R$ is the total fractional coverage of the redox-active species and $\nu$ is the number of water molecules replaced by one adsorbed molecule. F, R and T are the Faraday constant, universal gas constant and absolute temperature, respectively. The signs of the effective lateral interaction parameter, $\nu G \theta_T$, the relationship between attractive and repulsive forces, the shape of the voltammogram and the full peak width at half peak height, $W^{1/2}\left(= \frac{2RT}{nF}\left|\ln\left(\frac{1+\sigma}{1-\sigma}\right) - \nu G \theta_T \sigma\right|\right)$ being $\sigma = \sqrt{\frac{2-\nu G \theta_T}{4-\nu G \theta_T}}$ ,of the electrochemical wave are summarized in Table 1.

Applying this approach, we fitted the experimental current-potential profiles of FcC6SH modified Au(111) substrates using *M* different contributions by *M* independent Laviron-type functions [50], assuming that they were additive. The expression for the total current-potential profiles is then:

$$i_{\text{Total}} = \left(\frac{F^2}{RT}\right) n^2 v A \Gamma_T \sum_{j=1}^{M} B_j \left[\frac{f_j\left(1-f_j\right)}{1-2\left(\nu G \theta_T\right)_j f_j\left(1-f_j\right)}\right] \quad (4)$$

where the potential dependence is expressed by the following equation [50]:

$$n\left(E - E_{\text{peak},j}\right) = \frac{RT}{F}\left[\ln\left(\frac{f_j}{1-f_j}\right) + \left(\nu G \theta_T\right)_j \left(1-2f_j\right)\right] \quad (5)$$

where $B_j$ is the amplitude parameter and $E_{\text{peak},j}$ is the peak potential of the *j*-contribution. In the fitting procedure, the parameters $\left(\nu G \theta_T\right)_j$, $B_j$ and $E_{\text{peak},j}$ for each *j*-

contribution were used as adjustment parameters (i.e. this fitting function (Eq. (4)), has 3*M*adjustment parameters to describe *M* different contributions). The potential dependence of $f_j$ (Eq. (5)) was solved numerically using a modification of the Powell hybrid method [60–62].

Wandlowski and co-workers [52] identified three different adsorption regions represented by three separate Laviron-type functions (*M* = 3) for FcC11SH modified Au (111), Au (100) and Au (110) substrates. The correlation between the experimental and theoretical anodic profiles were excellent. On the other hand, Yu and co-workers [53] used only two contributions (*M* = 2) with poorer fitting results. Finally, Cao and co-workers [16] analysed the experimental anodic profiles of FcC6SH modified gold beads using the $W^{1/2}$ to calculate $\nu G \theta_T$.

*3.2. General SECM Model*

For a SECM feedback experiment, the complete dependence of $i_T$ normalized respect to its value at infinite distance ($I_T = i_T / i_{T,\infty}$) on $E_S$ and *d* normalized respect to the tip radius ($L = d/a$) has been recently reported [55]. This dependence is given by Eq. (6).

$$I_T(E_S, L) = \left(\frac{4\beta L}{\pi}\right)\left[I_T^{PF}(L) - I_T^{NF}(L)\right] I_{TLC}(E_S, L) + c(E_S, L, t) I_T^{NF}(L) \qquad (6)$$

The core of this equation is the normalized TLC current ($I_{TLC} = i_{TLC} / i_{T,\infty}$) for the reaction that flows between the tip disk microelectrode and an identical area at the substrate ($A_{TLC} = \pi a^2$). In addition, this equation involves the positive and negative feedback normalized limiting currents ($I_T^{PF}$ and $I_T^{NF}$, respectively), a correction factor $\beta$ due to the finite tip-sheath radius ($r_g$) that depends on the ratio $R_g = r_g / a$ [63], and the dimensionless concentration $c = C(L)/C^*$, where $C(L)$ and $C^*$ are concentrations of the tip reactant at distance $L$ and in the bulk solution, respectively. Both the

$I_{TLC}(E_S, L)$ and the $c(E_S, L, t)$ dependences must be solved for the particular reaction and substrate configuration that is analysed.

*3.3. Modelling the adsorbed FcC6SH molecules in a TLC*

On the basis of previous models for adsorbed FcC6SH monolayer on gold substrates that take into account the electrochemical responses of pinholes [64,65] and of the monolayer [47], we propose as a first approximation that the substrate modification can be represented in the TLC configuration by a heterogeneous surface with two different electrocatalytic activities (see Scheme 1). Then, the whole TLC current is the addition of two independent TLC contributions. The pinholes are represented as an ensemble of uniform nanodisks with radius $r_{pin}$ randomly dispersed on the substrate surface. The reaction proceeds with current densities $j_{pin}$ (on the pinholes) and $j_{ML}$ (on the monolayer). Note that this model does not take into account the diffusion through the pinhole thickness [65] and the presence of collapsed regions around the defects [44]. It also oversimplifies the well-known heterogeneity in shape and size of the defects [4] by assuming a disk geometry and a mean value for the radius. The TLC current for this modified substrate is expressed by the following equation:

$$I_{TLC} = \frac{j_{pin} A_{pin} + j_{ML} A_{ML}}{i_{T,\infty}} \qquad (7)$$

where $A_{pin} = N\pi r_{pin}^2$, being $N$ the number of pinholes, and $A_{ML} = A_{TLC} - A_{pin} = \pi\left(a^2 - N r_{pin}^2\right)$ are the surface areas occupied by the pinholes and the monolayer, respectively. In terms of the fraction of pinholes or of uncovered area ( $f_{pin} = A_{pin}/A_{TLC} = N R_{pin}^2$, where $R_{pin} = r_{pin}/a$), $I_{TLC}$ is defined by Eq. (8):

$$I_{TLC}(E_S, L) = f_{pin} I_{pin}(E_S, L) + \left(1 - f_{pin}\right) I_{ML}(E_S, L) \qquad (8)$$

where $I_{pin} = j_{pin}\left(\pi a^2/i_{T,\infty}\right)$ and $I_{ML} = j_{ML}\left(\pi a^2/i_{T,\infty}\right)$.

Both TLC regions define their own limiting current densities. For the monolayer, as long as it covers most of the surface ( $f_{pin} < 0.5$ ), the limiting current density should be

equivalent to that of a simple linear TLC, which leads to $I_{L,ML}(L)=\left(4\beta L/\pi\right)^{-1}$. Moreover, for the pinholes a model that combines linear and radial diffusion can be used [66], which leads to $I_{L,pin}(L)=\left(R_{pin}/f_{pin}+4\beta L/\pi\right)^{-1}$.

*3.3.1. Reaction rate on the pinhole*

In general, the reaction at the pinholes is faster than it is at the monolayer [47], and it can be reversible as it will be discussed later with our experiments. The TLC expression for a reversible reaction [54,67], $I_{pin}(E_S,L)$ is defined by:

$$I_{pin}(E_S,L)=\left(\frac{1}{1+\Theta}\right)\left(\frac{R_{pin}}{f_{pin}}+\frac{4\beta L}{\pi}\right)^{-1} \tag{9}$$

where $\Theta=\exp\left[F\left(E_S-E^0\right)/RT\right]$ and $E^0$ is the formal potential of the probed electrode reaction. Moreover, the reversible reaction at the pinholes controls the concentration profile of tip reactant around the substrate surface over the shielding potential range. Then, the term $c(E_S,L,t)$ in Eq. (6) that results for serial linear and radial diffusion at the proposed pinhole ensemble model is given by Eq. (10):

$$c(E_S,L,t)=\left(\frac{1}{1+\Theta}\right)\left[1+\frac{4L\Theta}{\pi f_{pin}\left(R_{pin}+4\sqrt{\tau}\right)}\right] \tag{10}$$

where $\tau\left(=Dt/\pi a^2\right)$ is the normalized time.

A more general treatment considering a quasi-reversible reaction at the pinholes is only justified when experimental evidence shows a clear deviation from a reversible behaviour. In such a case, equations for $I_{pin}(E_S,L)$ and $c(E_S,L,t)$ for quasi-reversible kinetics [67] can be straightforwardly obtained.

*3.3.2. Reaction rate on the monolayer surface:*

As it was discussed in the Introduction section, the electron transfer through the hydrocarbon chains of the redox functionalized monolayer to the redox mediator in solution may proceed via direct electron tunnelling (det) and via mediated electron transfer (met) through bimolecular reaction of the redox moieties [43]. Then, the TLC

current through the monolayer can be written in terms of the normalized reaction rates ( $V = va/DC^*$ ) of these two parallel processes ($V_{ML}^{\text{det}}$ and $V_{ML}^{\text{met}}$, respectively) as:

$$I_{ML}\left(E_S, L\right) = \left(\frac{\pi}{4\beta}\right)\left[V_{ML}^{det}\left(E_S, L\right) + V_{ML}^{met}\left(E_S, L\right)\right] \tag{11}$$

A Butler-Volmer type dependence can be adopted for the direct electron tunnelling rate, so the $V_{ML}^{det}\left(E_S, L\right)$ dependence in terms of the normalized tunnelling rate constant ( $\Lambda_{\text{det}} = k_{\text{det}} a/D$ ) and of the charge transfer coefficient ( $\alpha$ ) results according to Eq. (12).

$$V_{ML}^{det}\left(E_S, L\right) = \Lambda_{\text{det}} \Theta^{-\alpha}\left[1 - \left(\frac{4\beta}{\pi}\right) I_{ML}(E_S, L)\left(1 + \Theta\right) L\right] \tag{12}$$

On the other hand, the mediated mechanism involves the electron tunnelling through the monolayer to/from the adsorbed redox moiety (previously studied by cyclic voltammetry) and the bimolecular electron transfer between adsorbed and diffusing species at the monolayer|solution interface [43]. By following the same previous treatment that uses the Laviron approach [50,51] to describe the electron transfer of the adsorbed species as a reversible process with a Frumkin-type isotherm (see Section 3.1), but only considering a single type of site, together with an irreversible model for the bimolecular reaction, it results the $V_{ML}^{met}\left(E_S, L\right)$ dependence given by Eq. (13).

$$V_{ML}^{met}\left(E_S, L\right) = \Lambda_{met} e^{-2\nu\theta_T a_{RR}} \theta_T \left(1 - f\right) e^{\nu G \theta_T f}\left[1 - \left(\frac{4\beta}{\pi}\right) I_{ML}(E_S, L) L\right] \tag{13}$$

where *f* is the fraction of the total coverage due to O and its potential dependence is expressed by Eq. (3), considering that $E = E_S$ and $n = 1$.

These equations involve not only the adsorption parameters of the Laviron-type approach ($\nu G \theta_{\text{T}}, a_{OO}, a_{RR}, a_{OR}, E_{\text{peak}}$) [50], but also the normalized bimolecular reduction rate constant ($\Lambda_{met} = k_{red} a/D$). The irreversible approximation given by Eq. (13) is valid either when $E_S << E_{\text{peak}}$ or when $k_{red}$ is much larger than the backward

(oxidation) bimolecular rate constant [43]. Finally, by introducing Eqs. (12) and (13) into Eq. (11), the complete $I_{ML}(E_S, L)$ dependence given by Eq. (14) is obtained:

$$I_{ML}(E_S, L) = \left(\frac{4\beta}{\pi}\right) \frac{\left[\Lambda_{met} e^{-2\nu\theta_T a_{RR}} \theta_T (1-f) e^{\nu G \theta_T f} + \Lambda_{det} \Theta^{-\alpha}\right]}{1 + L\left[\Lambda_{met} e^{-2\nu\theta_T a_{RR}} \theta_T (1-f) e^{\nu G \theta_T f} + \Lambda_{det} \Theta^{-\alpha} (1+\Theta)\right]} \tag{14}$$

## 4. Results and discussion

### *4.1. Cyclic voltammetry*

#### *4.1.1. Successive potential scans*

Figure 1 shows the voltammograms (expressed as the current density, *j* ) of FcC6SH modified Au(111) substrates performed in 1.00 M $HClO_4$registeredat 0.050 $Vs^{-1}$for different cycles (2 and 10). The experiments were carried out with different FcC6SH modified Au(111) substrates prepared using the same dipping procedure regarding concentration, time and solvent. It is important to mention that the first potential scan was not included in the analysis because the current-potential profiles greatly varied from sample to sample (see Supplementary Material). Hence, the voltammograms were analysed from the second potential scan. Clearly, the shapes of the voltammograms measured in the second cycle also strongly depend on the Au(111) substrates used for the modification. However, the difference becomes less evident after ten cycles. The measured voltammograms were identical between the sixth and tenth cycles for all the cases studied. These six voltammograms exemplify the behaviour of three representative families of electrochemical signals measured with different Au(111) substrates modified with FcC6SH. The three families show two signals between 0.30 V and 0.45 V during the second anodic cycle, in agreement with published results[28,68]that show multi-peak voltammograms of FcC6SH modified gold substrate measured in $HClO_4$. In family I, these signals are clearly separate whereas, in the other two cases, the lower potential signal appears as a shoulder (family II) or overlapped (family III) with the second signal. On the other hand, a single oxidation signal was recorded for the three families from cycle 6 up to 10. When analysing the reduction profiles, the electrochemical signal appears between 0.29 V and 0.34 V and remains constant during cycling.

In order to understand such a behaviour, the electrochemical oxidation profiles were fitted using Eq. (4). Figure 2 shows the experimental and fitted anodic scans (after subtracting the baseline) corresponding to the second and tenth cycles for the three families together with the contributions given by the independent Laviron-type functions. The results of the fitting procedure related to cycles 3-9 for family I are shown in the Supplementary Material. Contrary to recent reported results of anodic responses of FcC6SH on gold beads measured in 0.1 M $Na_2SO_4$ [16], three functions were the minimal set (making up more than 90% of the total electrochemical signal) needed for the deconvolution of the voltammograms of each family shown in Fig. 1. Table 2 gives the main fitting parameters considered in the model for these contributions: the effective lateral interactions parameter ($(\nu G\theta_{\mathrm{T}})_j$), the full peak width at half peak height ($W_j^{1/2}$), and the oxidation peak potential ($E_{\mathrm{peak},j}$). The charge fractions ($q_j/q_{\mathrm{Total}}$) calculated from fitting the experimental electrochemical signal are also reported in the table. The total charge density, calculated by integrating the oxidation signal, does not depend (within the limits of experimental error) on the cycle or family analysed. The calculated values are (35 ± 3) μC $cm^{-2}$, (31 ± 3) μC $cm^{-2}$ and (26 ± 3) μC $cm^{-2}$ for families I, II and III, respectively. Therefore, the change in the shape of the voltammograms with cycling is not related to the adsorbed amount of FcC6SH.

The effect of successive potential scans on the shape of the electrochemical signals of the FcC6SH monolayer on Au(111) substrate was analysed for the three families. The extremely sharp and narrow peak current observed at 0.30 V for family I in the second scan (Fig. 2a) contributes around 20% of the total charge. In this contribution the attractive interactions between adsorbed molecules prevails (see Table 1). Narrow

current peaks (spikes) have been already observed with FcC6SH and FcC11SH monolayers on gold substrate under certain conditions [28,52]. In fact, the calculated $W_j^{1/2}$ for this contribution fully agrees with the reported value. This narrow electrochemical signal gradually becomes less noticeable with successive cycles while a new current peak is defined at 0.60 V with Langmuir-type features (Fig. 2d). On the other hand, two signals contributing up to 80% of the total charge with different effective interactions appear at more positive potentials: A Langmuir-type contribution at 0.36 V and a wide and flat signal, representative of repulsive interactions, at 0.45 V. These signals are not affected by cycling the FcC6SH modified Au(111) substrates. Families II and III show similar behaviours in which the signal at around 0.30 V in the second cycle is less sharp and narrow than observed in family I. Thus, attractive interactions between adsorbed molecules are less important before cycling in these cases. The contributions at more positive potentials (0.45 V) behave in similar way as described for family I. As indicated by the experimental voltammograms, cycling the FcC6SH modified Au(111) substrate produces similar electrochemical responses. Therefore, the type of effective lateral interactions and the charge fraction of each contribution change during the cycling. These results indicate the coexistence of different domains of adsorbed FcC6SH molecules in the monolayer that are rearranged during cycling. Since these results clearly indicate the importance of cycling before performing any experimental measurement with FcC6SH modified Au(111) substrates, the following discussion is based on pre-treated substrates.

*4.1.2. Nature of the supporting electrolyte*

Figure 3 shows the voltammograms of FcC6SH modified Au(111) substrates performed in different electrolytes and scan rates whereas Figure 4 presents the respective

relationship between the peak current density and the scan rate. Considering that this substrate modification can be coupled to a bioelectrochemical device to improve its performance [12–16], the selected supporting electrolytes represent gradual modifications from the commonly used 1.00 M $HClO_4$ pH 0.2 in electrochemical determinations to the 0.10 M phosphate buffer (PB) pH 8.5, compatible with surface bioactivity[69–71].

Clearly, the shape of the voltammograms measured in 1.00 M $HClO_4$ does not depend on the scan rate. Thus, the FcC6SH monolayer, although heterogeneous, is stable against successive changes of the scan rate in the same electrolyte after the cycling pre-treatment. However, the shape of the electrochemical signals strongly depends on the nature and concentration of the supporting electrolyte as well as on the pH. As indicated by the linear relationship between the current density and the scan rate, this behaviour is not attributable to any desorption caused by the electrolyte or by cycling at different scan rates. The different slopes of these linear relationships also indicate that the shape of the voltammograms in a particular supporting electrolyte is due to the different effective lateral interactions and charge fraction of each contribution (see Eq. (4)). The effect of the nature of the electrolyte is also observed in the anodic and cathodic peak potentials. These values do not change with the scan rate but they depend on the nature and concentrations of the supporting electrolyte going from 0.39 V in $HClO_4$ to 0.50 V in PB for the anodic wave.

Figure 5 shows the experimental and fitted anodic scans (after subtracting the baseline) together with the contributions given by the independent Laviron-type functions corresponding to the electrochemical signals in different supporting electrolyte. Three functions were the minimal set (making up more than 90% of the total electrochemical signal) needed for the deconvolution of the experimental voltammograms of each signal

shown in Figure 3. Table 3 lists the values of $q_j/q_{\text{Total}}$, $E_{\text{peak},j}$ and $(\nu G\theta_{\text{T}})_j$. As expected, the scan rate does not affect the number, position or ratio of each contribution (Supplementary Material). Moreover, the calculated total charge densities for these systems are (31 ± 3) μC cm$^{-2}$, (26 ± 3) μC cm$^{-2}$ and (30 ± 3) μC cm$^{-2}$, for 1.00 M $NaClO_4$, 0.10 M $NaClO_4$ and PB, respectively, indicating that the supporting electrolyte does not affect the adsorbed amount of FcC6SH.

Even though three main contributions are also observed in 1.00 M $NaClO_4$, none of them have attractive lateral interactions and they are oxidized at more positive potentials than observed in 1.00 M $HClO_4$. The value of $(\nu G\theta_{\text{T}})_j$ in this supporting electrolyte tends to zero, indicating a Langmuir-like behaviour (Table 1). On the other hand, the contribution at about 0.45 V is not modified by the pH. These results show that the pH of the supporting electrolyte does not affect the heterogeneity of the monolayer on Au(111), although the interactions between adsorbed FcC6SH molecules change. When the electrolyte is less concentrated, there are again three major contributions with more positive $E_{\text{peak},j}$ values than those found with the experiments performed in 1.00 M $NaClO_4$. However, the contribution with repulsive lateral interactions becomes less significant. Hence, both the pH and the concentration of the supporting electrolyte modify the type of lateral interactions between adsorbed FcC6SH molecules. Changing the supporting electrolyte from $NaClO_4$ to PB, results in more pronounced changes both in the number of contributions and in the $(\nu G\theta_{\text{T}})_j$ parameters. In PB, there are two contributions that oxidize at the same potential, which is more positive than those found in the presence of $ClO_4^-$. The lateral interactions for one contribution are repulsive whereas for the other one, the parameter $(\nu G\theta_{\text{T}})_j$ tends to zero. This result is not

surprising recalling that not only the type of ions is changed but also that PB ions can be specifically adsorbed onto Au substrates [72–75].

As already mentioned, the shape of the anodic current-potential profile depends on the type of interactions between adsorbed Fc molecules, generating sharp signals before cycling only at acid pH. From a thermodynamics point of view, this behaviour could be due to ion pairing between the oxidized $Fc^+$ on the Au(111) substrate and the anion of the supporting electrolyte [26–32,40]. The formation of these ion pairs, favours the oxidation process of the adsorbed FcC6SH molecules at acid pH and high $ClO_4^-$ concentration. Hence, the oxidation of FcC6SH molecules at low potentials in $HClO_4$ is a cooperative process due to favourable interactions between the cationic adsorbed species and the supporting electrolyte anions. At intermediate potentials, the oxidation process does not depend on the pH, but it becomes less favourable when the concentration of the supporting electrolyte decreases. The same behaviour is observed with the domains of adsorbed FcC6SH molecules that oxidizes at higher potentials. The presence of phosphate ions in the buffer solution affects both ion pair formation and the metal substrate [72–75], resulting in two domains that oxidize at the same potential.

Finally, it is worth mentioning that the anodic current-potential profile has different information than the cathodic one. In general, two processes control the anodic current-potential profile: lateral interactions between adsorbed molecules and ion-pairing between $Fc^+$ moieties and the anions of the supporting electrolyte. Hence, the oxidation potentials are determined from the strength of the interaction between the adsorbed positive moieties and the negative ions present in solution. As a consequence, at least three domains with different oxidation potentials were observed by fitting the experimental profiles. On the other hand, the cathodic current-potential profile is mainly controlled by ion-pairing because at the switch potential all the oxidized $Fc^+$ moieties

interact with the anions of the supporting electrolyte. Thus, during the backward scan potential, the monolayer behaves as a homogeneous electrochemical system in such a way that $Fc^+$ moieties are reduced at the same potential. Consequently, the voltammetric analysis was restricted to the anodic current-potential profiles because they provide with relevant information to characterize the monolayer in terms of the different domains.

*4.2. Scanning Electrochemical Microscopy*

*4.2.1. Tip-substrate approach curves*

Figure 6 shows typical approach curves measured when a Pt tip oxidizing FcMeOH to $FcMeOH^+$, under diffusion control, was approached to a FcC6SH modified Au(111) substrate polarized at different $E_S$ to probe the reduction of the tip-generated $FcMeOH^+$ through the feedback loop. Significant feedback current is detected at all potentials up to 0.15 V, which results from the electron transfer by both or either one of the described pathways of electron transfer through the hydrocarbon chains and/or through pinholes. At $E_S$ > 0.15 V the shielding process [67]was evident. Moreover, curves measured at the most cathodic potentials ($E_S \leq -0.55\,\mathrm{V}$) were properly fitted with the total positive feedback dependence [63] indicating that the reaction at the substrate reaches total diffusion control at these potentials. Then, tip currents measured in total positive feedback conditions were used to estimate *d* values in the performed experiments.

*4.2.2 SECM polarization curves*

Figure 7 (a) shows the experimental $i_T$ as a function of $E_S$ curves (the so-called SECM polarization curves) for the reduction of tip-generated $FcMeOH^+$ ($E_T$ = 0.40 V)on FcC6SH modified Au(111) substrates acquired at different *d* values by slow

potentiodynamic scans (0.01 V $s^{-1}$) from –0.60 V to 0.40 V. In these potential range, the adsorbed Fc moieties change from the reduced to the oxidised state at around 0.2 V. The SECM polarization curves show two potential regions: $E_S < 0.20\,\mathrm{V}$ ,where the FcMeOH mediator is regenerated at the substrate leading to a positive feedback current and $E_S > 0.20\,\mathrm{V}$ ,where the substrate consumes FcMeOH competing with the tip. The most useful part of these curves (full of kinetic features) is the positive feedback region, where the SECM polarization curve increases as $L(=d/a)$ decreases. A qualitative inspection of the $i_T\left(E_S\right)$ dependence over this region shows a shoulder that becomes more pronounced as $L$ decreases, which is most likely caused by a mechanistic transition. A fast process occurs at $E_S < 0.22\,\mathrm{V}$ and seems to reach a limiting rate for $E_S < 0.10\mathrm{V}$. Considering that such response has been previously associated to the fast $FcMeOH^+$ reduction on pinholes or defects [47], the reaction on these regions was assumed reversible in our model. At more cathodic $E_S$ values ($< 0.05\mathrm{V}$), a second slower process is evident, which tends to reach a mass-transport limiting value only at $E_S < -0.50\,\mathrm{V}$. This is most likely caused by the electro-reduction of $FcMeOH^+$ on the monolayer. All these polarization curves were reproducible, and could be repetitively measured in spite of the very cathodic limit potential ($-0.6\,\mathrm{V}$) applied to the FcC6SH modified Au(111) substrate.

SECM polarization curves were normalized and correlated using Eq. (6) with the developed model, pointing to find a single set of kinetic and adsorption parameters. These correlations are shown in Figure 7(b), and the obtained parameters are listed in Table 4. For the correlations, the adsorption parameter $\nu G \theta_T$ was fixed at a value of -0.2, and $E_{peak}$ was fixed at 0.435 V ($E_{peak} - E^0$ = 0.23 V). These values are weighted

averages of the values measured by cyclic voltammetry in 0.1 M $NaClO_4$ solution previously listed in Table 3. In spite of the large number of correlated variables, fitting of all curves measured at different *L* values with a single set of parameters is a strong constrain that limits the possible solutions to a narrow group of values. For example, if the mediated reaction is assumed to occur with a null rate ($\Lambda_{met} = 0$), then the curves cannot be fitted with a single $f_{pin}$ value. Figure 8 shows the theoretical SECM polarization curves calculated with the parameters shown in Table 4 for two *L* values as well as the contribution of each electron transfer pathway to the whole response. The effects of the parallel electron transfer processes on the SECM polarization curves are evidenced on different potential regions. The pinholes ($I_{pin}(E_S)$) govern the response at $E_S - E^o > -0.10\text{V}$, as $I_{pin}$ quickly reaches a diffusional limiting rate. Notwithstanding, a contribution from the monolayer ($I_{ML}(E_S)$) is also detected over this potential range. The calculated $f_{pin}$ value of 0.29 indicates a high density of pinholes that causes a positive feedback current almost similar to the feedback current from the monolayer when *L* > 0.4 (see Figure 8 (b)). The resulting fittings are valid for any value of normalized pinhole mean size laying in the indicated range ($R_{pin} < 3\times10^{-3}$), so its estimated real value results not larger than 12 nm. As previously discussed, the electron transfer through the FcC6SH modified Au(111) substrate to the $FcMeOH^+$ mediator in solution may proceed by either direct or mediated electron transfer [43]. The monolayer contribution observed at $E_S - E^o > -0.10\text{V}$ is caused by the reaction via mediated electron transfer. On the other hand, the reaction via direct electron transfer controls the curve shape at the most cathodic potentials ($E_S - E^o < -0.10\,\text{V}$) before it reaches the diffusion limiting value.

Probably the most relevant kinetic parameter that resulted from this analysis is the transfer coefficient ($\alpha$) of the direct electron transfer process, mainly due to the implications that can be inferred from its value. An unusually small value of $\alpha$ was obtained from the correlations, similarly to what was observed in other reported studies [47,48]. As it was previously demonstrated by Finklea and co-workers [44], such behaviour evidences the presence of collapsed regions of the monolayer around the pinholes where the monolayer thickness varies. By doing numerical simulations these authors demonstrated that as the rate constant depends on many factors including monolayer thickness and structure [76,77]. The presence of diverse monolayer regions with different tunnelling rates leads to different dependences of the local current densities on potential [44]. Then the whole experimental current is in fact a convolution of many current-potential dependences, whose slope results much smaller than those of the monolayers with uniform thicknesses [44]. Thus, the apparent tunnelling rate constant that was measured in this work on the FcC6SH modified Au(111) substrate ( $\Lambda_{det} = 1.45$, which leads to $k_{det} = 0.025\,\mathrm{cm\,s^{-1}}$) is in fact a sort of mean value that results from a heterogeneous surface with a profile of rate constants following an arbitrary distribution function. An improved model should take this effect into consideration in order to fully address the influence of pinholes on the SECM responses and to calculate more reliable rate constant values.

Another interesting result is the poor effect of the parameter depicting the lateral interactions of adsorbed FcC6SH molecules, i.e. $\nu G \theta_T$, on the fitting quality of the measured SECM polarization curves. The correlations of these curves were totally insensitive to this parameter over $E_S - E^o$ < -0.2 V. Even though the cyclic voltammograms accounting for the oxidation process of the adsorbed FcC6SH molecules on Au(111) are strongly affected by lateral interactions, most of the $E_S$

values in the SECM experiments were cathodic enough respect to the peak potential that the substrate was essentially covered by the reduced Fc species. Then, the effect of $\nu G\theta_T$ on the fraction of the total coverage due to the $Fc^+$ molecules was negligible over most of the analysed potential range. In fact, an effect of the adsorption parameters ($\nu G\theta_T$ and $\nu a_{RR}\theta_T$) on the bimolecular reaction rate should be expected, according to Eq. (13), at less cathodic potentials, and the polarization curve should actually be affected by these parameters. However, the contribution of the interaction parameters to the mediated electron transfer rate is coupled to the rate constant, so any change of $\nu G\theta_T$ and of $\nu a_{RR}\theta_T$ in the correlation will be balanced by an opposite change of $\Lambda_{met}$. Then the actual value of $\Lambda_{met}$ cannot be separated from the contribution of the interaction parameters from these results.

## Conclusions

The two perspectives addressed in this work are very useful to acquire a complete overview of the different electron transfer pathways that take place on Fc-terminated alkanethiol monolayers on Au(111) substrates. In the first place, the integrated theoretical-experimental approach used to analyse the lateral interactions between adsorbed FcC6SH molecules from cyclic voltammetry, allows to understand the effect of the successive potential scans and different supporting electrolyte on the electrochemical behaviour of the modified substrates. Successive potential scans change the surface domains distribution and affect the oxidation process of the electroactive monolayer. As a consequence, the substrate modification becomes more homogeneous in such a way that potential scans can be used as a reliable pre-treatment procedure. Furthermore, ion-pair formation between the oxidized Fc moieties and the anions of the

supporting electrolyte controls the electron transfer processes as well as the type of the lateral interactions and the number of the surface domains.

In the second case, the correlation between SECM experiments and the TLC model using an additional redox mediator in solution allows to identify the pinholes contributions and the electron transfer kinetic parameters through direct and mediated pathways. The pinholes contribution behaves as an ensemble of nanodisks and takes place through a reversible electron transfer process. The mediated electron transfer pathway proceeds with an effective rate constant that is affected not only by the bimolecular rate constant but also by the lateral interaction parameter of the adsorbed electroactive species. Direct electron transfer through a tunnelling mechanism occurs at more cathodic potentials. The heterogeneity in the monolayer thickness, due to the collapsed regions around the pinholes, causes abnormally low transfer coefficient that may lead to an overestimated tunnelling rate constant.

**Acknowledgements**

J.L.F., S.A.D. and C.E.G. are Researchers from Consejo Nacional de Investigaciones Científicas y Tecnológicas (CONICET). M.F.S. thanks CONICET for the fellowship granted. Financial support from CONICET (PIP 2013 11220120100174 – PIP 2013 11220120100575), Secretaria de Ciencia y Tecnología de la Universidad Nacional de Córdoba (SECyT-UNC) and Fondo para la Investigación Científica y Tecnológica (FONCyT) PICT-2012-1820 and PICT-2012-0634 are gratefully acknowledged.

**References**

[1] A. Ulman, An Introduction to Ultrathin Organic Films From Langmuir-Blodgett to Self-Assembbly, Academic Press Inc, London, 1991.

[2] L.H. Dubois, R.G. Nuzzo, Annu. Rev. Phys. Chem. 43 (1992) 437–463.

[3] A. Ulman, Chem. Rev. 96 (1996) 1533–1554.

[4] J.C. Love, L.A. Estroff, J.K. Kriebel, R.G. Nuzzo, G.M. Whitesides, Chem. Rev. 105 (2005) 1103–1169.

[5] J.J. Calvente, R. Andreu, Curr. Opin. Electrochem. 1 (2017) 22–26.

[6] A.L. Eckermann, D.J. Feld, J.A. Shaw, T.J. Meade, Coord. Chem. Rev. 254 (2010) 1769–1802.

[7] S.E. Creager, L.A. Hockett, G.K. Rowe, Langmuir 8 (1992) 854–861.

[8] J. Shao, E.A. Josephs, C. Lee, A. Lopez, T. Ye, ACS Nano 7 (2013) 5421–5429.

[9] C.E.D. Chidsey, Science 251 (1991) 919–922.

[10] J.F. Smalley, S.W. Feldberg, C.E.D. Chidsey, M.R. Linford, M.D. Newton, Y.-P. Liu, J. Phys. Chem. 99 (1995) 13141–13149.

[11] D. Nkosi, J. Pillay, K.I. Ozoemena, K. Nouneh, M. Oyama, Phys. Chem. Chem. Phys. 12 (2010) 604–613.

[12] J. Liu, M.N. Paddon-Row, J.J. Gooding, J. Phys. Chem. B 108 (2004) 8460–8466.

[13] B. Kazakevičiene, G. Valincius, G. Niaura, Z. Talaikyte, M. Kažemekaite, V. Razumas, D. Plaušinaitis, A. Teišerskiene, V. Lisauskas, Langmuir 23 (2007)

4965–4971.

[14] M. Mir, A.T.A. Jenkins, I. Katakis, Electrochem. Commun. 10 (2008) 1533–1536.

[15] M. Antuch, D.G. Abradelo, R. Cao, New J. Chem 386 (2014) 386–390.

[16] M. Antuch, D.G. Abradelo, R. Cao, Electroanalysis (2015) 1939–1943.

[17] Y. Lee, B. Carsten, L. Yu, Y. Lee, B. Carsten, L. Yu, (2009) 1495–1499.

[18] R. Dasari, F.J. Ibañez, F.P. Zamborini, Langmuir 27 (2011) 7285–7293.

[19] N. Nerngchamnong, L. Yuan, D.-C. Qi, J. Li, D. Thompson, C.A. Nijhuis, Nat. Nanotechnol. 8 (2013) 113–118.

[20] H. Jeong, D. Kim, G. Wang, S. Park, H. Lee, K. Cho, W.T. Hwang, M.H. Yoon, Y.H. Jang, H. Song, D. Xiang, T. Lee, Adv. Funct. Mater. 24 (2014) 2472–2480.

[21] H. Jeong, Y. Jang, D. Kim, W.T. Hwang, J.W. Kim, T. Lee, J. Phys. Chem. C 120 (2016) 3564–3572.

[22] H. Jeong, D. Kim, D. Xiang, T. Lee, ACS Nano 11 (2017) 6511–6548.

[23] J.N. Israelachvili, Intermolecular and Surface Forces, Secod Ed, Academic Press Inc, London, 1992.

[24] A.S. Viana, A.H. Jones, L.M. Abrantes, M. Kalaji, J. Electroanal. Chem. 500 (2001) 290–298.

[25] H.C. De Long, D.A. Buttry, Langmuir 6 (1990) 1319–1322.

[26] H.C. De Long, J.J. Donohue, D.A. Buttry, Langmuir 7 (1991) 2196–2202.

[27] G.K. Rowe, S.E. Creager, Langmuir 7 (1991) 2307–2312.

[28] K. Uosaki, Y. Sato, H. Kita, Langmuir 7 (1991) 1510–1514.

[29] W.R. Fawcett, J. Electroanal. Chem. 378 (1994) 117–124.

[30] R. Andreu, J.J. Calvente, W.R. Fawcett, M. Molero, Langmuir 13 (1997) 5189–5196.

[31] M. Ohtani, S. Kuwabata, H. Yoneyama, Anal. Chem. 69 (1997) 1045–1053.

[32] M. Ohtani, Electrochem. Commun. 1 (1999) 488–492.

[33] H. Ju, D. Leech, Phys. Chem. Chem. Phys. 1 (1999) 1549–1554.

[34] T. Kondo, M. Okamura, K. Uosaki, J. Organomet. Chem. 637–639 (2001) 841–844.

[35] G. Valincius, G. Niaura, B. Kazakevičienė, Z. Talaikytė, M. Kažėmėkaitė, E. Butkus, V. Razumas, Langmuir 20 (2004) 6631–6638.

[36] X. Yao, J. Wang, F. Zhou, J. Wang, N. Tao, J. Phys. Chem. B 108 (2004) 7206–7212.

[37] G. Filippini, F. Goujon, C. Bonal, P. Malfreyt, Soft Matter 7 (2011) 8961–8968.

[38] Y. Yokota, T. Yamada, M. Kawai, J. Phys. Chem. C 115 (2011) 6775–6781.

[39] E.R. Dionne, T. Sultana, L.L. Norman, V. Toader, A. Badia, J. Am. Chem. Soc. 135 (2013) 17457–17468.

[40] K. Nguyen, E.R. Dionne, A. Badia, Langmuir 31 (2015) 6385–6394.

[41] S.E. Creager, G.K. Rowe, J. Electroanal. Chem. 420 (1997) 291–299.

[42] G. Filippini, Y. Israeli, F. Goujon, B. Limoges, C. Bonal, P. Malfreyt, J. Phys. Chem. B 115 (2011) 11678–11687.

[43] B. Liu, A.J. Bard, M. V. Mirkin, S.E. Creager, J. Am. Chem. Soc. 126 (2004) 1485–1492.

[44] H.O. Finklea, S. Avery, M. Lynch, T. Furtsch, Langmuir 3 (1987) 409–413.

[45] K.S. Alleman, K. Weber, S.E. Creager, J. Phys. Chem. 100 (1996) 17050–17058.

[46] K.B. Holt, Langmuir 22 (2006) 4298–4304.

[47] A. Kiani, M.A. Alpuche-Aviles, P.K. Eggers, M. Jones, J.J. Gooding, M.N. Paddon-Row, A.J. Bard, Langmuir 24 (2008) 2841–2849.

[48] S. Amemiya, in:, A.J. Bard, M. V. Mirkin (Eds.), Scanning Electrochem. Microsc., 2nd Ed., CRC Press (Boca Raton), 2012, pp. 127–156.

[49] N. Moradi, A. Noori, M.A. Mehrgardi, M.F. Mousavi, Electroanalysis 28 (2016) 823–832.

[50] E. Laviron, J. Electroanal. Chem. 52 (1974) 395–402.

[51] E. Laviron, J. Electroanal. Chem. 100 (1979) 263–270.

[52] A. V Rudnev, K. Yoshida, T. Wandlowski, Electrochim. Acta 87 (2013) 770–778.

[53] H. Tian, Y. Dai, H. Shao, H.Z. Yu, J. Phys. Chem. C 117 (2013) 1006–1012.

[54] C.G. Zoski, C.R. Luman, J.L. Fernández, A.J. Bard, Anal. Chem. 79 (2007) 4957–4966.

[55] M.A. Brites Helú, J.L. Fernández, J. Electroanal. Chem. 784 (2017) 33–40.

[56] H.L. Bonazza, J.L. Fernández, J. Electroanal. Chem. 650 (2010) 75–81.

[57] W. Haiss, D. Lackey, J.K. Sass, K.H. Besocke, J. Chem. Phys. 95 (1991) 2193–2196.

[58] G. Jarzabek, Z. Borkowska, Electrochim. Acta 42 (1997) 2915–2918.

[59] A.S. Baranski, P. Norouzi, Can. J. Chem. 75 (1997) 1736–1749.

[60] A.M. Ostrowski, Solution of Equations and System of Equations, 2sd Ed, Academic Press Inc, 1966.

[61] W.H. Press, S.A. Teukolsky, I.T. Vetterling, B.P. Flannery, Numerical Recipes in Fortran 77 The Art of Scientific Computing, 2nd Ed, Cambridge University Press, 1992.

[62] Subroutines Fortran Are Free Available Http//www.netlib.org (2017).

[63] C. Lefrou, R. Cornut, ChemPhysChem 11 (2010) 547–556.

[64] F. Fardad, A.J. Bard, M. V. Mirkin, Isr. J. Chem. 37 (1997) 155–163.

[65] G. Che, Z. Li, H. Zhang, C.R. Cabrera, J. Electroanal. Chem. 453 (1998) 9–17.

[66] C. Amatore, J.M. Savéant, D. Tessier, J. Electroanal. Chem. 147 (1983) 39–51.

[67] C.G. Zoski, J.C. Aguilar, A.J. Bard, Anal. Chem. 75 (2003) 2959–2966.

[68] G.K. Rowe, S.E. Creager, Langmuir 10 (1994) 1186–1192.

[69] L.E. Valenti, V.L. Martins, E. Herrera, R.M. Torresi, C.E. Giacomelli, J. Mater. Chem. B 1 (2013) 4921.

[70] E. Herrera, C.E. Giacomelli, Colloids Surf. B. Biointerfaces 117 (2014) 296–302.

[71] E. Herrera, J. Valdez Taubas, C.E. Giacomelli, Appl. Surf. Sci. 356 (2015) 679–686.

[72] M.W. Hsiao, R.R. Adzic, E.B. Yeager, Electrochim. Acta 37 (1992) 357–363.

[73] G. Niaura, A.K. Gaigalas, V.L. Vilker, J. Phys. Chem. B 101 (1997) 9250–9262.

[74] M. Weber, I.R. De Moraes, A.J. Motheo, F.C. Nart, Colloids Surfaces A Physicochem. Eng. Asp. 134 (1998) 103–111.

[75] F. Silva, A. Martins, J. Electroanal. Chem. 467 (1999) 335–341.

[76] K. Weber, L. Hockett, S. Creager, J. Phys. Chem. B 101 (1997) 8286–8291.

[77] P.K. Eggers, D.B. Hibbert, M.N. Paddon-Row, J.J. Gooding, J. Phys. Chem. C (2009) 8964–8971.

**Figure captions:**

**Figure 1.** Cyclic voltammograms of FcC6SH modified Au(111) substrates performed in 1.00 M $HClO_4$ at 0.050 $Vs^{-1}$ for cycles 2 (——) and 10 (——) for the three representative families of electrochemical signals found when modifying the substrate with the same dipping procedure (Fc concentration: 1.00 mM, time: 15 h and solvent: $CH_2Cl_2$).

**Figure 2.** Experimental and fitted anodic scans of FcC6SH modified Au(111) substrates performed at 0.050 $Vs^{-1}$ in 1.00 M $HClO_4$ for cycles 2 ((a)-(c)) and 10 ((d)-(e)) for the three representative families shown in Fig. 1 and the contributions calculated from independent Laviron-type functions (Eq. (4)). Different contributions (solid lines), experimental (●) and simulated (——) total anodic current-potential profile.

**Figure 3.** Cyclic voltammograms of FcC6SH modified Au(111) substrates performed in different electrolytes: (a) 1.00 M $HClO_4$, (b) 1.00 M $NaClO_4$, (c) 0.10 M $NaClO_4$ and (d) 0.10 M phosphate buffer (PB) and scan rates: (——) 0.005; (——) 0.010; (——) 0.050; (——) 0.100 and (——) 0.150 V $s^{-1}$ after the substrate pretreatment.

**Figure 4.** Current density as function of the scan rate for the oxidation reaction of FcC6SH modified Au(111) substrates performed in different electrolytes: (●) 1.00 M $HClO_4$, (●) 1.00 M $NaClO_4$, (●) 0.10 M $NaClO_4$ and (●) 0.10 M phosphate buffer (PB).

**Figure 5.** Experimental and fitted anodic scans of FcC6SH modified Au(111) substrates performed at 0.050 $Vs^{-1}$ in different electrolytes: (a) 1.00 M $HClO_4$, (b) 1.00 M $NaClO_4$, (c) 0.10 M $NaClO_4$ and (d) 0.10 M phosphate buffer (PB) for the data shown in Fig. 3 and the contributions calculated from independent Laviron-type functions (Eq. (4)). Different contributions (solid lines), experimental (●) and simulated (——) total anodic current-potential profile.

**Figure 6.** Approach curves for the reduction of $FcMeOH^+$ mediator (in 1 mM FcMeOH - 0.1 M $NaClO_4$ solution) of a Pt tip on FcC6SH modified Au(111) substrates polarized at different substrate potentials ($E_S$): –0.60 (a), –0.40 (b), 0.00 (c), 0.10 (d), 0.15 V (e).

Symbols represent the fitting of curve (a) with the theoretical total positive feedback dependence [63] ($E_T$ = 0.40 V, $i_{T,\infty}$ = 0.87 nA, $a$ = 4.1 μm, $R_g (= r_g / a) = 5$ ).

**Figure 7.** (a) Experimental SECM polarization curves for tip-generated $FcMeOH^+$ (in 1 mM FcMeOH - 0.1 M $NaClO_4$ solution) on FcC6SH modified Au(111) substrates at different tip-substrate distances. (b) Theoretical dependences (open symbols) resulting from correlations of normalized SECM polarization curves (solid lines) using Eq. (6) and parameters listed in Table 4. $L(=d/a)$ = 0.288 (i), 0.366 (ii), 0.407 (iii), 0.477 (iv), 0.620 (v) ( $E_T$ = 0.40 V, $i_{T,\infty}$ = 0.87 nA, $a$ = 4.1 μm, $R_g$ = 5).

**Figure 8.** Theoretical SECM polarization curves (dashed lines) and the contribution of each electron transfer route to the whole response given by the monolayer (——) and the pinholes (——) simulated with the parameters shown in Table 4 for $L$ = 0.288 (a) and 0.620 (b).

**Scheme 1:**

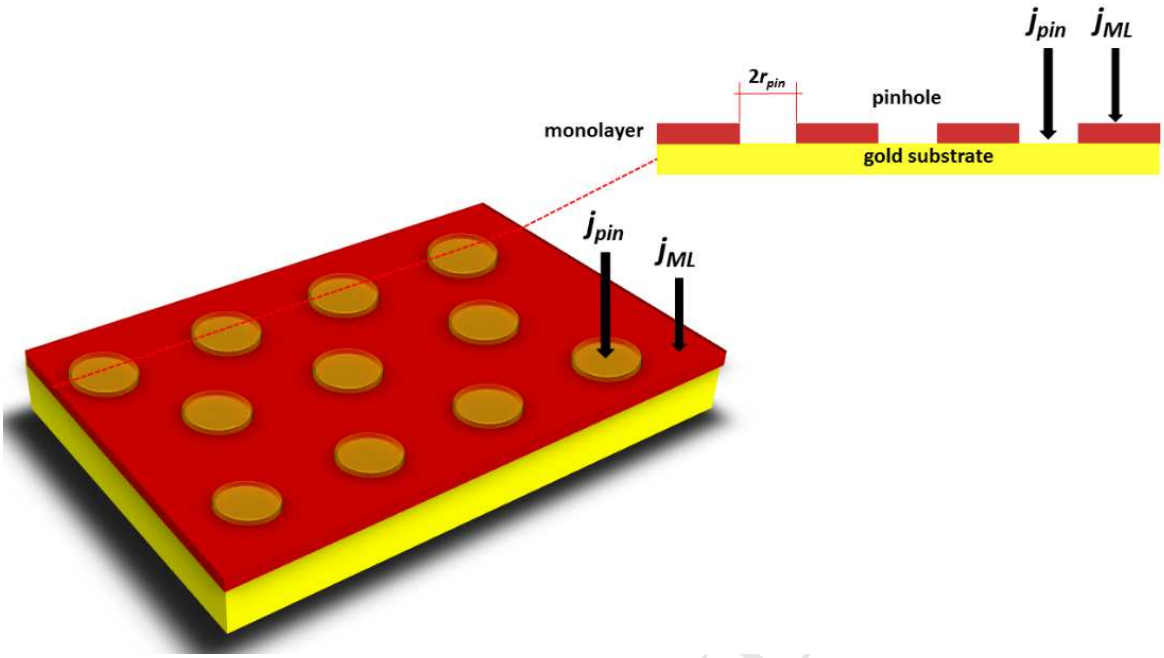

**Table 1:**

| $\nu G \theta_T$ | **Balance of forces** | **Shape of the voltammogram** | $nW^{1/2}$/ **V** |
|---|---|---|---|
| $=0$ | Attraction and repulsion forces compensate each other. | Langmuir-type adsorption. Independent of the total coverage. | 0.091 |
| $<0$ | Repulsion forces predominate. | Current peak becomes wider and flatter, with a more rounded shape. | >0.091 |
| $>0$ | Attraction forces predominate. | Current peak becomes narrower and sharper, when the total coverage increases. | < 0.091 |

**Table 2:** Fitting parameters considered in the model (Eq. (4)) for the different contributions of the anodic current-potential profiles of FcC6SH monolayers on Au(111) performed in 1.00 M $HClO_4$ at 0.050 $Vs^{-1}$: the effective lateral interactions parameter( $(\nu G \theta_T)_j$ ), the full peak width at half peak height( $W_j^{1/2}$ ), and the oxidation peak potential ( $E_{peak,\,j}$ ). Charge fractions ( $q_j/q_{Total}$ ) were calculated from fitting the experimental electrochemical signal.

| | Second cycle | | | | Tenth cycle | | | |
|---|---|---|---|---|---|---|---|---|
| Family | $(\nu G \theta_T)_j$ | $W_j^{1/2}$ / V | $E_{peak,\,j}$ / V | $q_j/q_{Total}$ | $(\nu G \theta_T)_j$ | $W_j^{1/2}$ / V | $E_{peak,\,j}$ / V | $q_j/q_{Total}$ |
| **I** | 1.5 | 0.02 | 0.30 | 0.19 | 1.0 | 0.04 | 0.31 | 0.13 |
| | –0.3 | 0.10 | 0.36 | 0.43 | –0.1 | 0.10 | 0.36 | 0.45 |
| | –2.3 | 0.22 | 0.45 | 0.36 | –2.2 | 0.21 | 0.44 | 0.35 |
| | ---- | ---- | ---- | ---- | –0.6 | 0.12 | 0.62 | 0.06 |
| | | | | | | | | |
| **II** | –0.5 | 0.12 | 0.36 | 0.06 | 0.7 | 0.05 | 0.33 | 0.04 |
| | –0.3 | 0.10 | 0.45 | 0.44 | –0.2 | 0.10 | 0.42 | 0.49 |
| | –3.9 | 0.31 | 0.45 | 0.43 | –3.5 | 0.28 | 0.43 | 0.39 |
| | –0.9 | 0.14 | 0.68 | 0.05 | –0.9 | 0.14 | 0.64 | 0.07 |
| | | | | | | | | |
| **III** | 0.0 | 0.09 | 0.31 | 0.15 | 0.0 | 0.09 | 0.31 | 0.17 |
| | –0.1 | 0.10 | 0.38 | 0.51 | 0.0 | 0.09 | 0.36 | 0.59 |
| | –1.5 | 0.17 | 0.46 | 0.31 | –0.9 | 0.14 | 0.47 | 0.21 |

**Table 3:** Fitting parameters considered in the model (Eq. (4)) for the different contributions of the anodic current-potential profiles of FcC6SH monolayers on Au(111) performed in different electrolytes at 0.050 $Vs^{-1}$: the effective lateral interactions parameter ($(\nu G\theta_T)_j$), and the oxidation peak potential ($E_{peak,j}$). Charge fractions ($q_j/q_{Total}$) were calculated from fitting the experimental electrochemical signal.

| Contribution | Fitting parameters | 1.00 M $HClO_4$ | 1.00 M $NaClO_4$ | 0.10 M $NaClO_4$ | 0.10 M phosphate buffer |
|---|---|---|---|---|---|
| 1 | $q_1/q_{Total}$ | 0.15±0.03 | | | |
| | $E_{peak,1}$ / V | 0.32±0.05 | | | |
| | $(\nu G\theta_T)_1$ | 0.4±0.1 | | | |
| 2A | $q_{2A}/q_{Total}$ | 0.35±0.05 | 0.30±0.05 | 0.75±0.05 | |
| | $E_{peak,2A}$ / V | 0.39±0.05 | 0.38±0.02 | 0.41±0.02 | |
| | $(\nu G\theta_T)_{2A}$ | –0.2±0.1 | –0.10±0.05 | –0.10±0.05 | |
| 2B | $q_{2B}/q_{Total}$ | | 0.25±0.05 | 0.15±0.05 | 0.45±0.05 |
| | $E_{peak,2B}$ / V | | 0.45±0.02 | 0.48±0.02 | 0.52±0.02 |
| | $(\nu G\theta_T)_{2B}$ | | –0.10±0.05 | –0.10±0.05 | –0.3±0.1 |
| 3 | $q_3/q_{Total}$ | 0.45±0.05 | 0.35±0.05 | 0.10±0.05 | 0.50±0.05 |
| | $E_{peak,3}$ / V | 0.45±0.05 | 0.46±0.02 | 0.58±0.02 | 0.52±0.02 |
| | $(\nu G\theta_T)_3$ | –2.0±0.5 | –1.5±0.5 | –1.0±0.5 | –2.2±0.5 |

**Table 4.** Parameter resulting from the correlations shown in Figure 7(b). Other involved parameters: $E^o = 0.205\,V$ (estimated from the tip voltammogram, see Supplementary Material), $E_{peak} - E^o = 0.23\,V$ (estimated from the substrate voltammogram in 0.1 M $NaClO_4$, see Supplementary Material), $\nu G\theta_T \cong -0.2$, $\tau = 10^3$.

| ***Pinholes*** | | ***Monolayer*** | | |
|---|---|---|---|---|
| $R_{pin}$ | $f_{pin}$ | $\Lambda_{met}\theta_T e^{-2\nu\,\theta_T a_{RR}}$ | $\Lambda_{det}$ | $\alpha$ |
| $< 3\times10^{-3}$ | 0.29 | 0.497 | 1.45 | 0.175 |

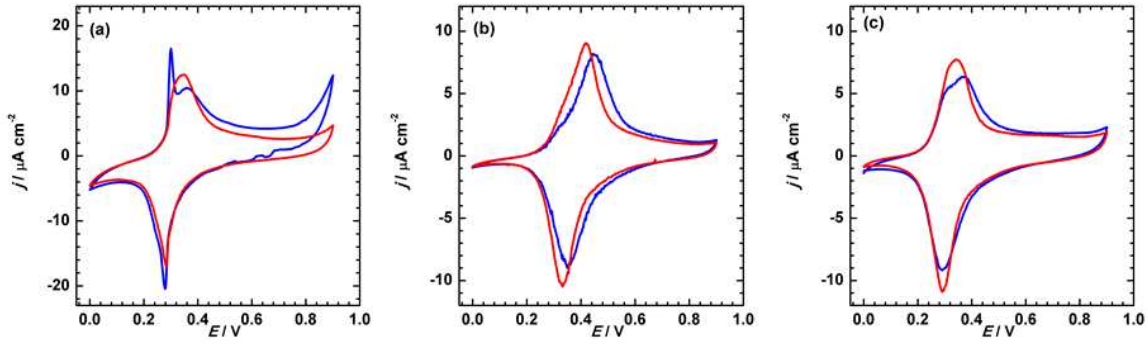

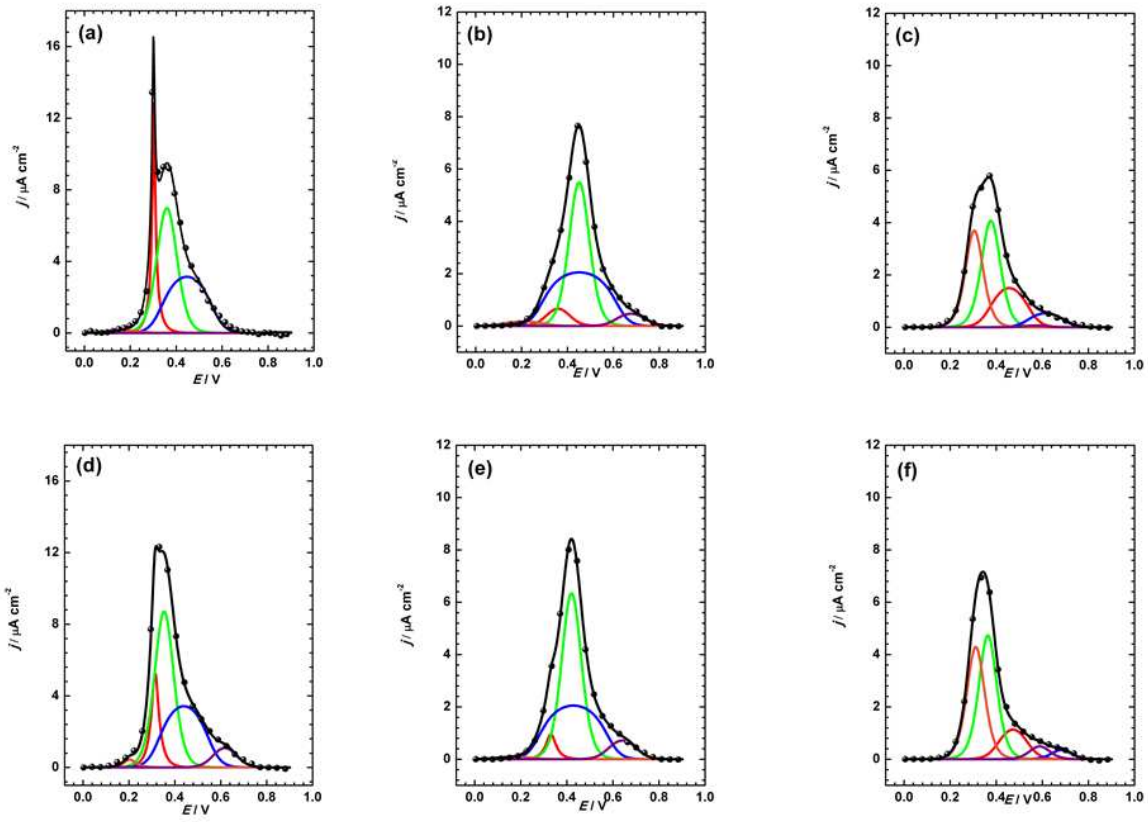

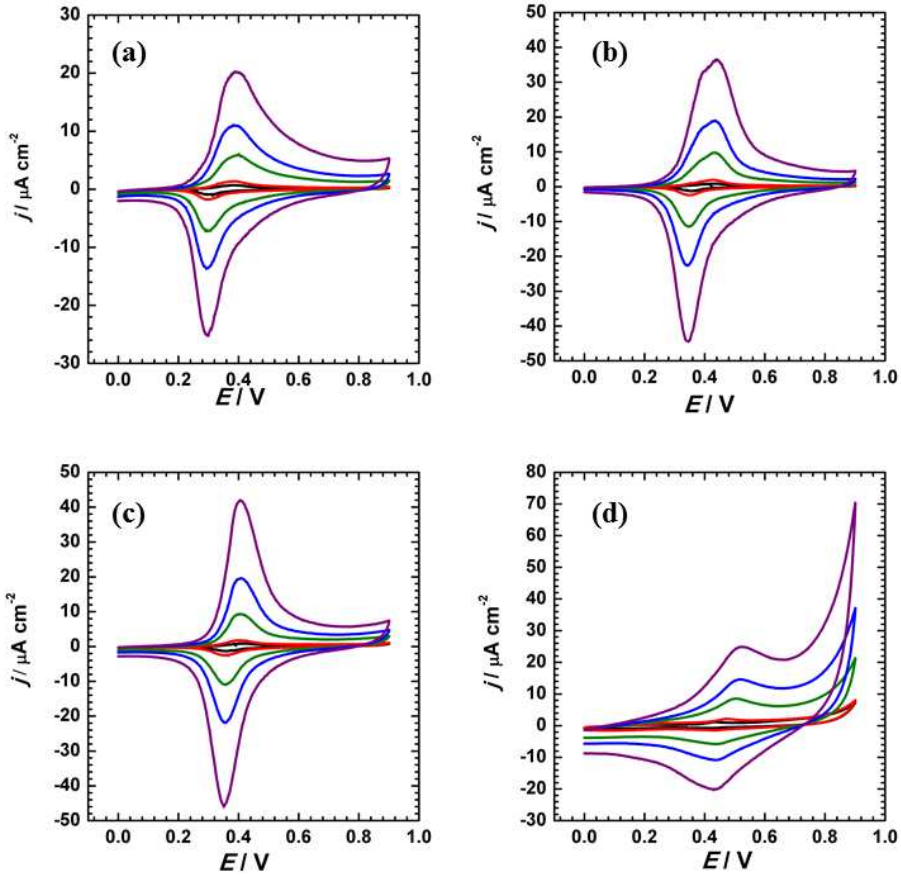

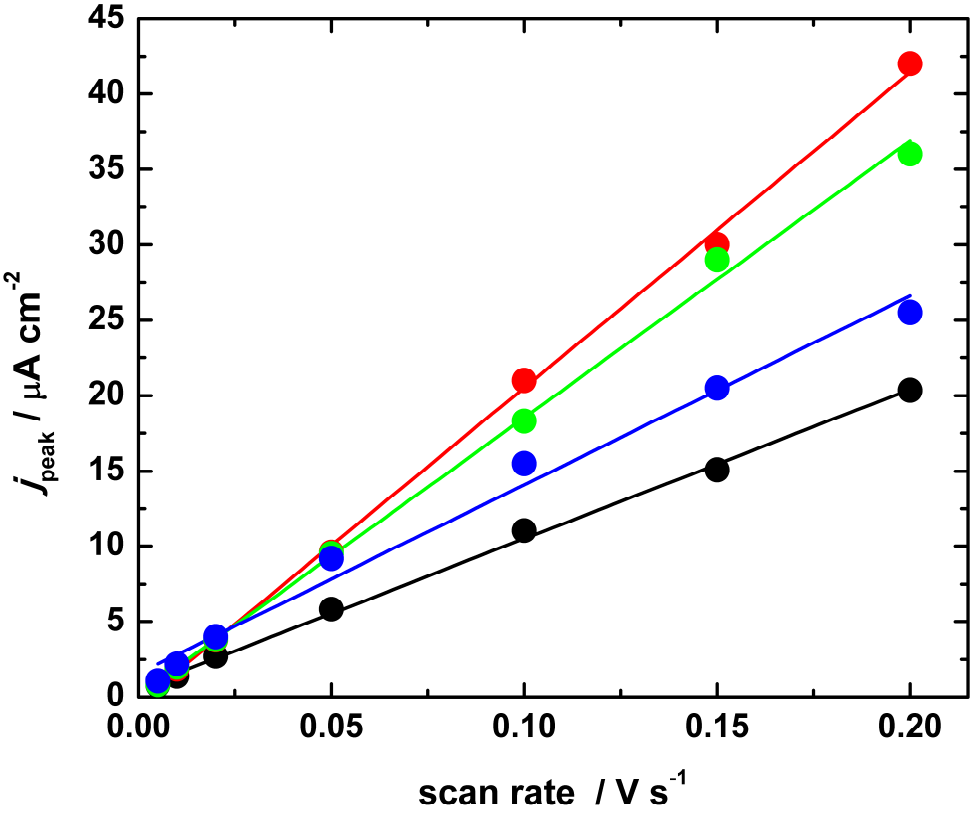

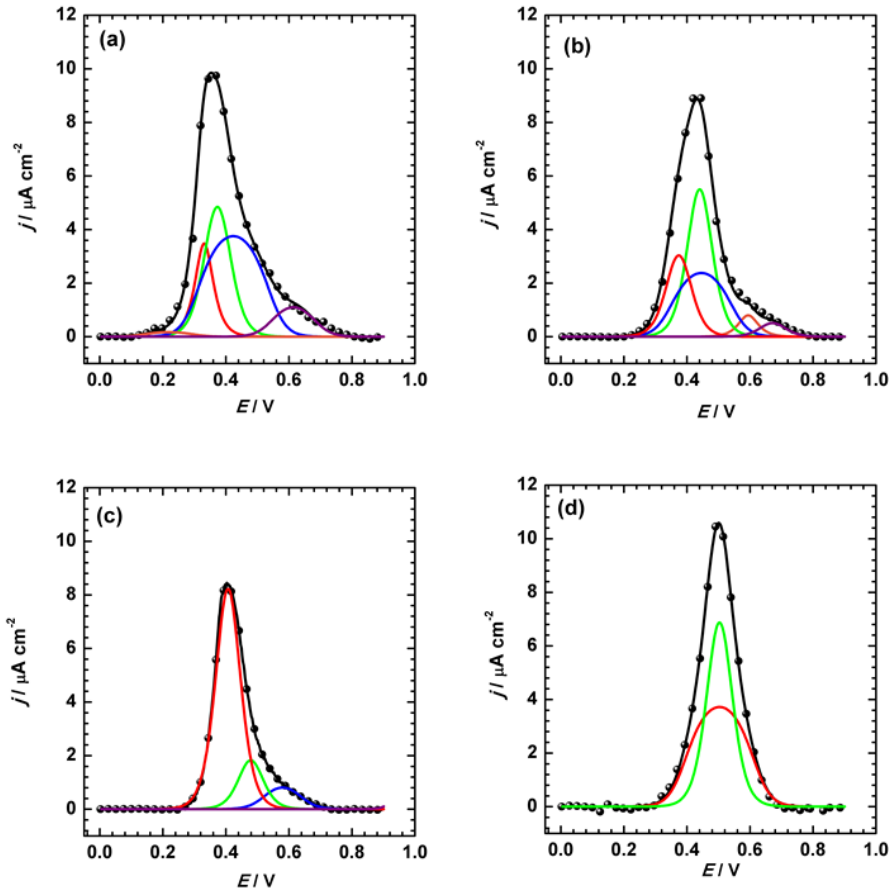

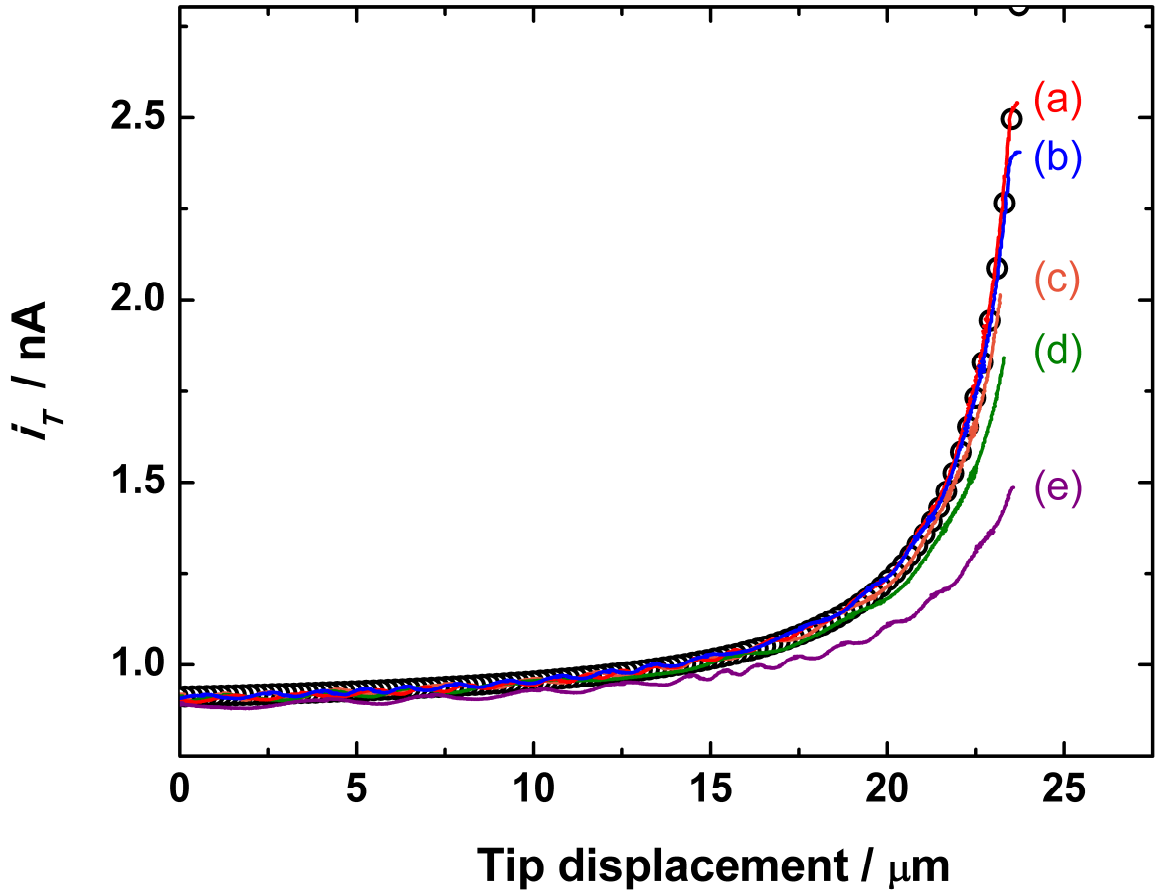

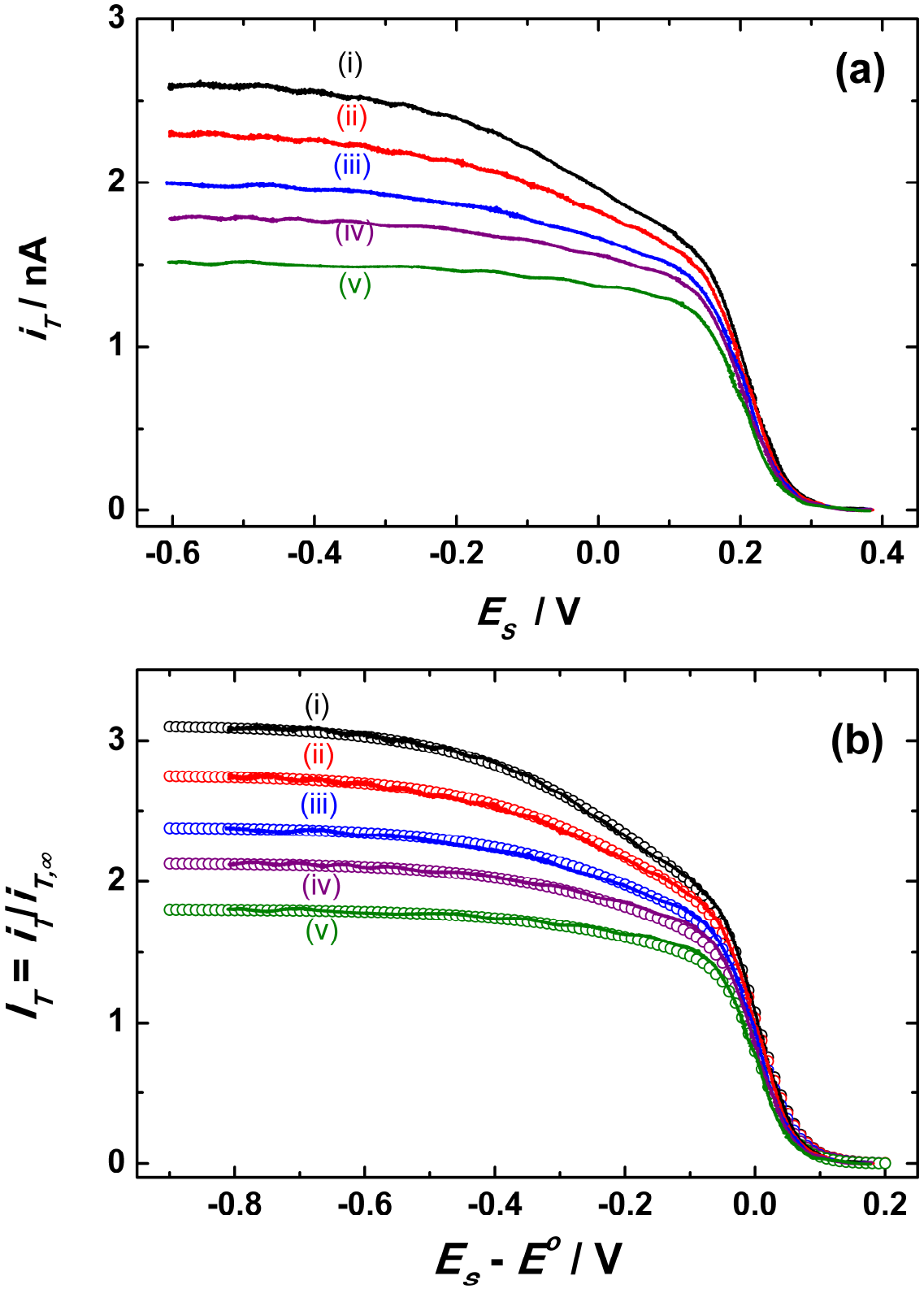
(a)
(i)
(ii)
(iii)
(iv)
(v)
$i_T$ / nA
$E_s$ / V
(b)
$I_T = i_T / i_{T,\infty}$
$E_s - E^o$ / V

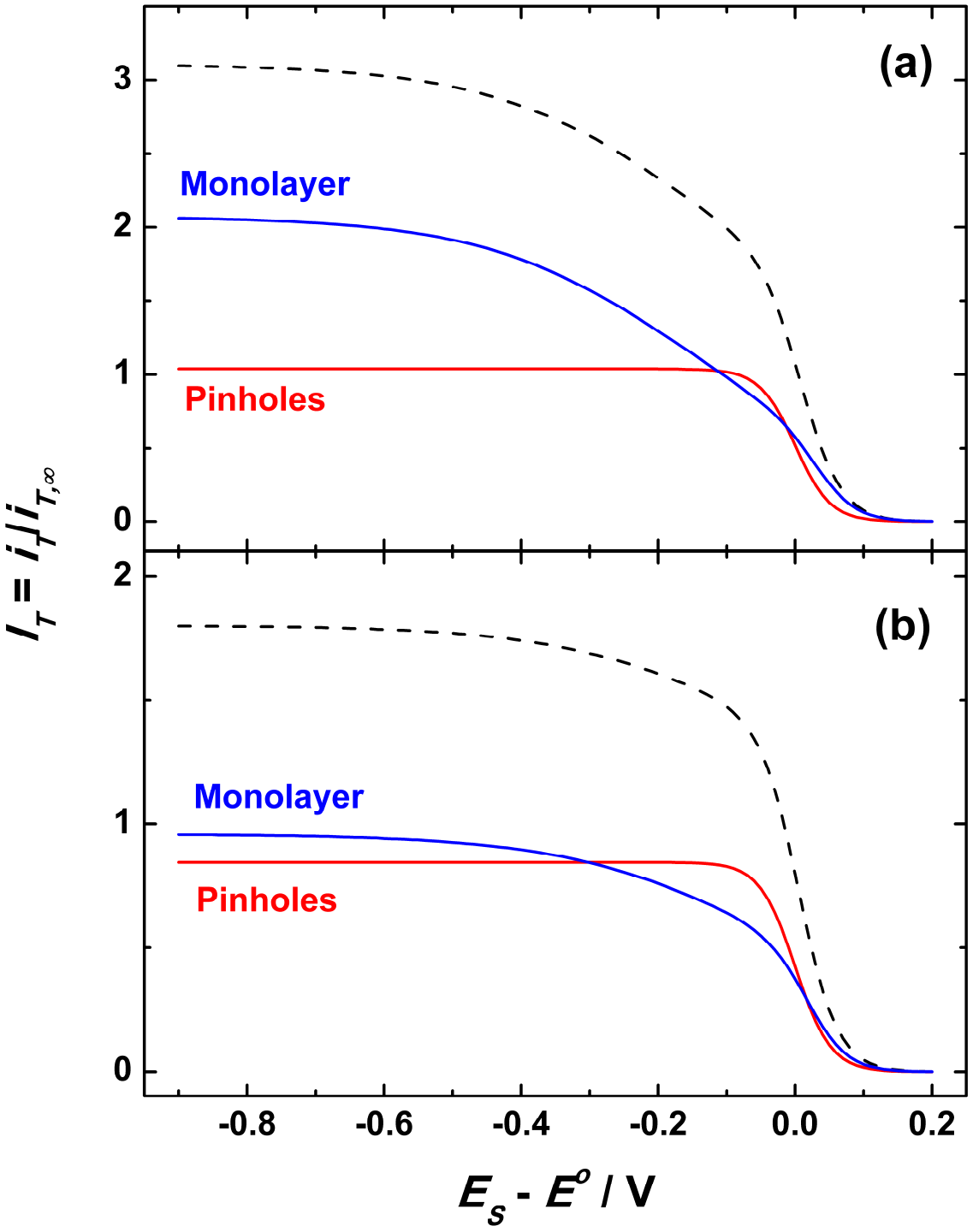
(a)
Monolayer
Pinholes
(b)
Monolayer
Pinholes
3
2
1
0
2
1
0
-0.8
-0.6
-0.4
-0.2
0.0
0.2
$I_T \equiv i_T / i_{T,\infty}$
$E_s - E^o$ / V

**Highlights**

> Electrochemical techniques to understand the electron transfer of adsorbed ferrocene are employed.

> Theory to understand the electron transfer of adsorbed ferrocene is developed.

> Monolayer and pinholes are incorporated into the SECM model.